Frascati Physics Series Vol. 74 (2022) ISBN: 978-88-86409-76-6
Frontier Objects in Astrophysics and Particle Physics
September 25- October 1, 2022

NEW PHYSICS SEARCH IN HIGH PRECISION MEASUREMENTS: THE MUON $g-2$ FACTOR

Marco Incagli
Istituto Nazionale di Fisica Nucleare (INFN) – Pisa
for the E989 (Muon $g-2$) experiment at Fermilab

Abstract

The Fermilab Muon g-2 experiment measures the muon anomalous magnetic moment with high precision. Together with recent improvements on the theory front, the first results of the experiment confirm the long-standing discrepancy between the experimental measurements and the Standard Model predictions. The observed value of $a_\mu(\text{FNAL}) = 116\,592\,040(54) \times 10^{-11}$ (0.46 ppm), combined with the previous experimental measurement, results in a discrepancy of $(251 \pm 59) \times 10^{-11}$ with the theoretical prediction, corresponding to 4.2 σ. This note presents the first results, the current status and the future prospects of the Muon g-2 experiment at Fermilab.

1 The g-factor and the muon magnetic anomaly

The g factor relates the magnetic moment of a particle to its angular momentum and charge-to-mass ratio.. For a charged lepton, g relates its magnetic moment

to its spin:

$$\vec{\mu} = -g\frac{e}{2m}\vec{S}. \tag{1}$$

Experimentally, it was found that $g = 2$, but only in 1928 this value was derived by Dirac starting from his famous formula. A spectacular success of the Quantum Theory.

The *magnetic anomaly* is the fractional difference of g from the value 2: $a = \frac{g-2}{2}$. Experimental evidence that $g \neq 2$ began mounting by 1947 through measurements such as the Lamb shift [1)] and preliminary measurements of g factors in gallium by Kusch and Foley [2)] indicating an incomplete understanding of electrodynamics at atomic scales. These and other results drove Schwinger, Feynman, Tomonaga and others to combine electromagnetism with the quantum theory and thereby provide the foundation of Quantum Electrodynamics (QED). QED predicted the possibility for charged particles to emit and reabsorb particles from the quantum vacuum, thus modifying the effective coupling constants. This manifestly quantum effect enhances the g factor to a value larger than 2, resulting in a non-zero anomaly. The famous Schwinger term, published in 1948,

$$a = \frac{\alpha}{2\pi} \sim 0.00116, \tag{2}$$

provides the leading contribution to the muon and electron magnetic anomaly[1]. Earlier that same same year, Kusch and Foley [3)], studying the Zeeman effect in Gallium atoms, published their definitive measurement of a non-null value of the magnetic anomaly for the elctron, finding

$$a^{exp} = 0.00119 \pm 0.00005. \tag{3}$$

Schwinger's prediction aligned in perfect agreement with the measurement and together they confirmed the existence of these *radiative corrections*. Another important success of QED.

Since then, many more diagrams contributing to a_μ have been evaluated. These include the theoretical *tour de force* of the QED contributions to 5 loops (12,672 diagrams) and the important weak interaction contributions. Many efforts have contributed to the evaluation of the QCD contributions in the

[1]Higher order contributions depend on the mass and thus are different for the two leptons

report of the Muon g-2 Theory Initiative (see [4] and references therein). Their consensus value of

$$a_\mu^{theo} = (116,591,810 \pm 43) \times 10^{-11}, \tag{4}$$

corresponding to 370 parts per billion (ppb), represents an impressive precision.

Similarly, the average of the published result [5] by the E989 collaboration (*Fermilab* $g-2$) and the previous value published by the E821 collaboration [6] at Brookhaven National Laboratory (BNL) yields the experimental value,

$$a_\mu^{exp} = 116,592,061 \pm 41) \times 10^{-11} \tag{5}$$

corresponding to 350 ppb. Theory and experiment show a difference of $(251 \pm 59) \times 10^{-11}$, which corresponds to 4.2 standard deviations. This difference can hide additional terms which are not accounted for by the current Standard Model of Particle Physics. As discussed in section 5, a recent lattice calculation of the QCD contribution to a_μ [7] reduces this discrepancy. The value presents a 2.2σ tension with the current theoretical determination, as reported in [4], therefore it is going through a close scrutiny within the theoretical community.

2 The muon $g-2$ strategy

The storage ring measurement of the muon anomaly relies on the spin precession and cyclotron motion of a charged particle orbiting in a uniform magnetic field. For a particle with momentum and spin vectors in a plane perpendicular to $\vec{B}$, a classical calculation of the difference of these frequencies yields

$$\omega_a = \omega_s - \omega_c = g\frac{e}{2m}B - \frac{e}{m}B = a_\mu \frac{e}{m}B \tag{6}$$

so that

$$a_\mu = \frac{\omega_a}{B}\frac{m}{e} \tag{7}$$

A relativistic calculation modifies the expression for ω_s and ω_c, but the difference in Eq. 6 remains unaffected. Thus, for $a_\mu = 0$, that is $g = 2$, the two vectors rotate with the same frequency, while for $a_\mu > 0$, the spin vector rotates faster than the momentum vector (see fig. 1). In the Fermilab $g-2$ setup, the spin advances by approximately 12^o with respect to the momentum each orbit. An observable sensitive to this relative precession rate would therefore provide a direct measurement of a_μ. This approach can be realized using a beam of

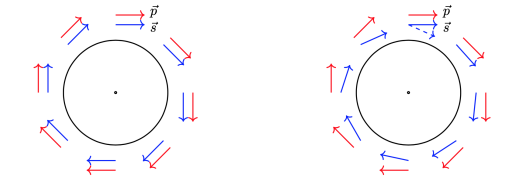

(a) $g = 2$: the muon spin and momentum vectors remain parallel.

(b) $g > 2$: the dashed blue arrow is the spin vector after one turn.

Figure 1: Spin and momentum vectors for a muon orbiting in a magnetic field (a) when $a_\mu = 0$, so the spin does not rotate relatively to the muon momentum, and (b) when $g > 2$.

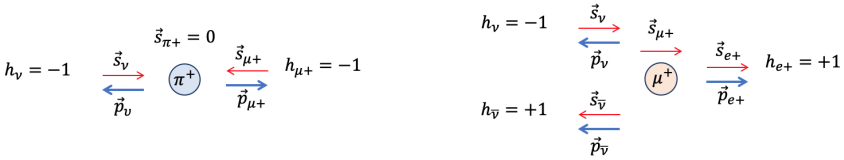

Figure 2: Schematic representation of pion (left) and muon (right) decays. Blue arrows ($\vec{p}$) and red arrows ($\vec{s}$) represent the momentum and spin vector, respectively, while h is the particle helicity.

polarized muons that evolve in a very stable and precisely measured magnetic field. Parity violation from the V-A structure of weak decays provides both a source of polarized muons and a way to statistically identify the muon spin direction (see fig. 2).

Storage of the muon beam requires vertical focusing from a quadrupole system, but the complicated spin precession in magnetic quadrupoles would render precision measurement impossible. The experiment therefore employs electrostatic quadrupoles. The electric field adds a $\vec{\beta} \times \vec{E}$ term, corresponding to a $\vec{B}$ field in the muon rest frame, to the expression in Eq. 6. With an "out of plane" (vertical) momentum component also considered, the spin evolves as [8]:

$$\frac{d(\hat{\beta} \cdot \vec{S})}{dt} = -\frac{q}{m} \vec{S}_T \cdot \left[a_\mu \hat{\beta} \times \vec{B} + \beta \left(a_\mu - \frac{1}{\gamma^2 - 1} \right) \frac{\vec{E}}{c} \right] \tag{8}$$

where $\vec{S}_T = \vec{S} - (\hat{\beta} \cdot \vec{S})\hat{\beta}$ is the spin component perpendicular to the momentum direction $\hat{\beta}$. With $\vec{E} = 0$ and the spin and momentum restricted to a plane

perpendicular to $\vec{B}$, Eq. 8 reduces to the simple Eq. 6.

Farley, Picasso and collaborators [9] realized in the 70s that the strategic choice of $\gamma = \sqrt{(a_\mu + 1)/a_\mu} \sim 29.3$ corresponding to a muon momentum $p_0 = 3.094$ GeV/c, would minimize the electric field contribution to ω_a. At this *magic momentum*, the prefactor of the $\vec{E}$ term vanishes. Because of the finite Storage Ring momentum acceptance of

$$\delta p/p = 0.15\%, \tag{9}$$

the cancellation occurs only at first order, but it allows treatment of the E-field contribution as a correction to the measured ω_a.

Utilizing comagnetometry Measurement of the magnitude of the field $|\vec{B}|$ by nuclear magnetic resonance (NMR) probes, as detailed in the next section, allows its expression in terms of the precession frequency of protons shielded in water $\tilde{\omega}'_p(T)$ as

$$\tilde{B} = \frac{\hbar\tilde{\omega}'_p(T)}{2\mu'_p(T)} = \frac{\hbar\tilde{\omega}'_p(T)}{2}\frac{\mu_e(H)}{\mu'_p(T)}\frac{\mu_e}{\mu_e(H)}\frac{1}{\mu_e}, \tag{10}$$

with the last three factors known precisely. The tilde in $\tilde{B}$ and $\tilde{\omega}'_p(T)$ indicates the average of the field over the muon distribution weighted by the detected decays over time. Combining Eqs. 6, 10, and $\mu_e = \frac{g_e}{2}\frac{e}{m_e}\frac{\hbar}{2}$ yields

$$a_\mu = \frac{\omega_a}{\tilde{\omega}'_p(T)}\frac{\mu'_p(T)}{\mu_e(H)}\frac{\mu_e(H)}{\mu_e}\frac{m_\mu}{m_e}\frac{g_e}{2}. \tag{11}$$

The Muon g-2 experiment thus provides the ratio

$$\mathcal{R}'_\mu = \frac{\omega_a \cdot (1 + C)}{\tilde{\omega}'_p \cdot (1 + B)} \tag{12}$$

as its primary experimental output, where C and B represent small corrections to the measured frequencies, related to beam dynamics (C) and to the presence of transient fields (B) as discussed in the next two sections.

The external factors – the ratio of the magnetic moment of a proton shielded in a spherical water sample at a reference temperature of $T = 34.7\,^\circ$C to the magnetic moment of an electron bound in hydrogen ($\mu'_p(T)/\mu_e(H)$), the ratio $\mu_e(H)/\mu_e$, the ratio of the muon to the electron mass and the g factor of the electron g_e – are known with a combined uncertainty of 25 ppb (see details in [5]).

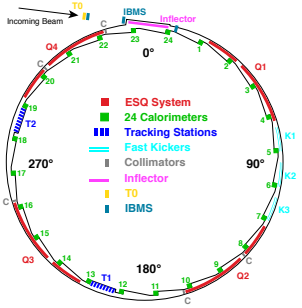

Figure 3: Layout of the Muon g-2 experiment at Fermilab

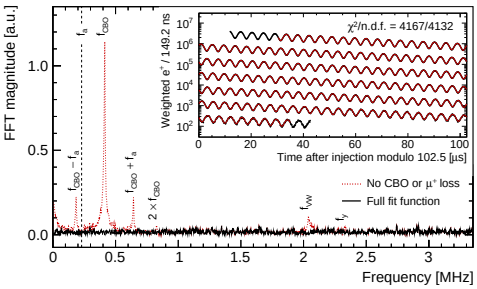

Figure 4: Fourier transform of the residuals from a fit following Eq. 13.

3 Measuring the anomalous precession frequency

The Fermilab complex delivers a sequence of 16 polarized muon bunches every 1.4 seconds to the Muon g-2 storage ring, where each bunch circulates for 700 μsec (a "fill"), about 11 muon lifetimes. A suite of 24 PbF_2 crystal calorimeters [10] situated uniformly around the interior of the storage ring (see Fig. 3) detect the positrons from beam muon decay. Every calorimeter consists of a 9×6 array of crystals, each with a Silicon Photomultiplier (SiPM) photodetector.

The variation of the positron energy spectrum as the spins in a monochromatic polarized muon beam precess leads to a rate time-dependence of the precession signal described by

$$N(t) = N_0 e^{-t/\gamma\tau_\mu}(1 + A(E_{thr}\cos(\omega_a t + \phi_{\rm ens})), \tag{13}$$

where γ is the standard boost factor (about 29.3 for muons at the magic momentum), τ_μ is the muon lifetime, ω_a is the anomalous precession frequency, and $A(E_{thr}$ is the asymmetry amplitude of the sinusoidal variation, which depends on the energy threshold applied to the detected positrons. The phase $\phi_{\rm ens}$ represents the ensemble average precession phase for the muons with detected daughter positrons. That average phase receives several contributions: the phase distribution within the injected beam, the longer drift distance for higher energy positrons vs lower energy positrons because of their different curvatures in the $\vec{B}$ field, and the detector acceptance as a function of the

transverse decay position of beam muons. Any effect correlated with time after beam injection that changes the makeup of muons with detected daughter positrons can lead to a time dependent drift $\phi_{\rm ens} \rightarrow \phi_{\rm ens}(t) \sim \phi_0 + \phi_1 t$. The latter term would directly bias the value of ω_a extracted from the data. A rate-dependent drift of the gains, for example, would change the effective energy threshold for detected positrons and lead to such a drift. A laser system [11] overlays well-characterized pulses on top of 10% of our muon fills that allow monitoring of and correction for such gain drifts. The pileup of positrons close in time and space in a calorimeter, whose probability varies as muons decay, can also lead to such a drift.

The collaboration utilizes two complementary techniques to reconstruct positron candidates from the waveforms, which bring different optimizations for resolving pileup. A third technique reconstructs the total measured energy versus time, which inherently eliminates bias from pileup. All told six independent analysis groups contributed 11 different measurements of ω_a (see [12]).

Fitting with only the basic decay model of Eq. 13 results in set of residuals that show distinct frequencies in their fast Fourier transform (FFT) shown in Fig. 4. These frequencies correspond to well-understood horizontal and vertical oscillations of the stored beam particles about their nominal circular orbits, which then couple to the acceptance of the detector system to modulate the observed rates. Appropriate modification of the basic model to account for these effects results in excellent quality fits that match the data well (see Fig. 4), have residuals with a featureless FFT spectrum, and χ^2 values consistent with the number of degrees of freedom. Combination of the four data subsets in Run-1, which correspond to different operating conditions, provides an overall statistical precision of 434 parts per billion (ppb).

Beam dynamics corrections The measured ω_a value requires three significant corrections to allow its interpretation as the frequency of Eqs. 7 or 11. The largest correction comes from the spread of stored muon energies in the beam, which results in imperfect suppression of the electric field term in Eq. 8. A second correction results from vertical momentum distribution of the beam muons, which alters the horizontal precession rate. A straw tracking system in the vacuum reconstructs the beam motion by extrapolation of the decay positrons back to the storage region. Finally, in Run-1 two faulty high voltage

resistors controlling the quadrupoles caused the beam to change shape and to slowly drift downward during the time interval used to determine ω_a. When coupled with acceptance effects, these changes resulted in a drift in the ensemble average phase, thus biasing ω_a. This effect has been modelled and understood well.

These corrections add up to a total shift $C \simeq 500$ ppb, with an uncertainty of 93 ppb, on the measured ω_a value as reported in the summary table 2.

4 The Magnetic Field $\tilde{\omega}'_p$

The 1.45 T field is generated by a *C*-shaped superconducting dipole magnet represented in figure 5. The magnetic field in the 4.5 cm radius storage region, described in detail in [13], is highly uniform in order to reduce the uncertainty on the determination of the field experienced by the muons. The uniformity is achieved by a long process of shimming that locally modifies the field direction. On top of this, an active feedback system modifies the coils current in order to keep the magnetic field stable, for example for hall temperature variations.

Tracking the magnetic field The magnetic field is measured by using pulsed proton Nuclear Magnetic Resonance (NMR) probes. A cylindrically shaped *trolley*, which can run on rails inside the storage region when muons are not present, hosts 17 NMR probes. Each probe is filled with petroleum jelly and the Larmor precession frequency of the protons within this jelly is measured. Each probe is carefully calibrated in terms of a precision calibration probe containing a pure water sample. The in-vacuum trolley runs in the Storage Ring and measures the magnetic field experienced by the muons in $\simeq 9000$ azimuthal locations.

The field's evolution between trolley runs is tracked by a set of 378 probes which are mounted in 72 azimuthal stations regularly spaced around the ring. The measurement from the trolley probes at a given azimuthal position θ, is determined by the solution of the source-free Laplace equation:

$$B = A_0 + \sum_{n=1} \left(\frac{r}{r_0}\right)^n [A_n \cos(n\theta) + B_n \sin(n\theta)] \tag{14}$$

expressed in polar coordinates (r, θ) with respect to the center of the muon ideal orbit, where $r_0 = 4.5$ cm is the radius of the storage region. The A_n

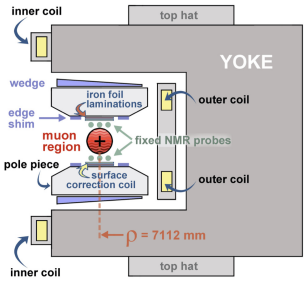

Figure 5: Cross section of the Muon $g-2$ magnet. It's a C-shaped superconducting magnet that provides a 1.45 T field.

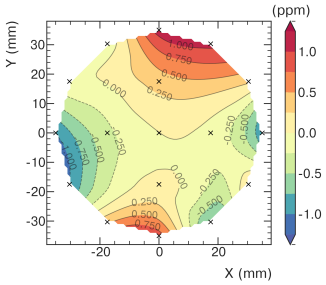

Figure 6: Relative variation of the magnetic field. The locations of the 17 trolley probes are indicated by (x).

and B_n parameters are the multipole strengths, also known as the normal and the skew multipole, respectively. The average over the azimuthal angle of the observed field, relative to the dominant dipole component, is shown in Fig. 6, together with the location of the measuring probes.

The fixed probes are used to track the field in between trolley runs.

Calibration procedure The trolley probes are calibrated by means of an external probe hosting a cylindrical water sample which is installed on a translation stage in the Storage Ring vacuum. The translation stage allows the calibration probe to be moved to each trolley probe position at a specific azimuthal location. The calibration and the trolley probes are then swapped several times to obtain a calibration constant for each of the 17 probes.

Muon weighting The magnetic field map has to be averaged over the muon transverse distribution at each azimuthal slice. The muon distribution is measured at $\sim 180^o$ and $\sim 270^o$ with respect to the injection point by two tracker stations. The in-vacuum straw tracker stations measure the trajectories of the decay positrons and trace them back to their radial tangency point within the storage ring. These profiles are propagated to other azimuthal locations using beam dynamics simulation.

Transient fields On top of the main static field, additional fields are induced by the fast switching storage ring elements that define the muon trajectory: the kicker and the electrostatic quadrupoles. An eddy current induced locally by the kicker system produces a transient magnetic field in the storage volume. A magnetometer, installed between the kicker plates, measures the Faraday rotation of a polarized laser light in a terbium-gallium-garnet (TGG) crystal. The second transient arises from charging the electrostatic quadrupoles, where the Lorentz forces induce mechanical vibrations in the plates that generate magnetic perturbations. Customized NMR probes measure these transient fields at several positions to determine the average field throughout the quadrupole volumes.

5 Result and perspectives

The recently published result [5] comprises four data subsets collected between April and July 2018 with distinct beam storage conditions, and totals 10^{10} positrons in the analysis. Table 1 lists the values of the muon and proton precession angular frequencies, ω_a and $\tilde{\omega}'_p$, for the four subsets along with the combined value for the ratio $\mathcal{R}'_\mu$. The systematic uncertainties correlate strongly among the four measurements, but the statitical term, which is uncorrelated among the subsets, dominates the total error. Combining $\mathcal{R}'_\mu$ with the external input in Eq. 7 yields a muon anomaly of

$$a_\mu(\text{FNAL}) = 116\,592\,040(54) \times 10^{-11} \quad (0.46\,\text{ppm}), \tag{15}$$

Table 2 summarizes the statistical and systematic contributions to the final result. The observed a_μ value is fully compatible with the previous BNL result, and combine to give an experimental average of

$$a_\mu(\text{Exp}) = 116\,592\,061(41) \times 10^{-11} \quad (0.35\,\text{ppm}). \tag{16}$$

The E989 experiment has already collected over 10 times the statistics used for this first measurement, and continues to collect additional data with the goal of reducing the statistical error to ~ 100 ppb. The systematic uncertainty currently sits at 157 ppb, a factor of 2 lower than in the previous BNL experiment. Work in progress should reduce this uncertainty down to the ~ 100 ppb level, which will allow E989 to reach its proposed total uncertainty goal

Run	$\omega_a/2\pi$ [Hz]	$\tilde{\omega}'_p/2\pi$ [Hz]	$\mathcal{R}'_\mu \times 1000$
1a	229081.06(28)	61791871.2(7.1)	3.7073009(45)
1b	229081.40(24)	61791937.8(7.9)	3.7073024(38)
1c	229081.26(19)	61791845.4(7.7)	3.7073057(31)
1d	229081.23(16)	61792003.4(6.6)	3.7072957(26)
			3.7073003(17)

Table 1: Run-1 group measurements of ω_a, $\tilde{\omega}'_p$, and their ratios $\mathcal{R}'_\mu$ multiplied by 1000.

Quantity	Correction (ppb)	Uncertainty (ppb)
ω_a^m (statistical)	–	434
ω_a^m (systematic)	–	56
C	500	93
$\langle \omega'_p(x,y,\phi) \times M(x,y,\phi) \rangle$	–	56
B	-44	99
Total external factors	–	25
Totals	544	462

Table 2: Summary table of uncertainties and corrections.

of a $\sigma^{tot} \sim 140$ ppb, a factor of 4 more precise than the previous experimental result.

Discussion The new result confirms the value of a_μ found previously by the BNL E821 experiment. The new world average shows a discrepancy of 4.2 standard deviations with the theoretical prediction recommended by the Muon g-2 Theory Initiative [4]. In April 2021, the Budapest-Marseille-Wuppertal (BMW) collaboration published a prediction of the QCD contribution to the muon anomaly based on lattice calculation [7]. This new prediction, which has a precision of 0.8%, more than a factor of two better with respect to the previous ones, hint at a reduced discrepancy with the observed anomaly. Recently, three other groups provided preliminary results on the same quantity measured in a reduced energy region, which accounts for ∼30% of the total correction due to QCD loops [15, 16, 17], all in agreement with the BMW value. This new prediction, however, is in tension with the current one, which is based on a dispersion integral of experimental $e^+e^- \to$ hadrons cross section

measurements [4]. As Ref. [14] notes, an increase in the measured hadronic cross section below $\sqrt{s} \sim 1$ GeV could reconcile the two predictions, although the required increase would be an order of magnitude larger than the current experimental precision. Additional contributions above ~ 1 GeV are excluded at the 95% Confidence Level as they result in tension with the prediction of fundamental parameters from the global electroweak fits, like the Higgs and W masses. Because of this, the theory community continues to push both calculational approaches to test the compatibility of different predictions in some detail. The tension that is now consolidating between the two theoretical approaches for the estimation of a_μ^{HVP} is being referred as *the new* $g-2$ *puzzle* and remains unexplained as of today.

Should the current a_μ prediction based on the dispersion integral hold, and assuming the current experimental central value also holds, the expected improvement in precision would ascertain the current discrepancy of 251×10^{-11} with an uncertainty in the $40 - 50 \times 10^{-11}$ range, which would provide strong evidence of physics beyond the Standard Model (BSM physics). Such a discrepancy, of the same order of magnitude as the electroweak contribution to a_μ (154×10^{-11}), would indicate a TeV scale for the BSM physics. Even if the prediction and experimental determination should agree in the end, the improvement in a_μ will provide a powerful constraint on any model extending the Standard Model. The next few years will provide exciting opportunities as the Muon g-2 experiment and the theory community continue to push on this precision frontier.

Acknowledgments

The Muon $g-2$ Experiment was performed at the Fermi National Accelerator Laboratory, a U.S. Department of Energy, Office of Science, HEP User Facility. Fermilab is managed by Fermi Research Alliance, LLC (FRA), acting under Contract No. DE-AC02-07CH11359. Additional support for the experiment was provided by the Department of Energy offices of HEP and NP (USA), the National Science Foundation (USA), the Istituto Nazionale di Fisica Nucleare (Italy), the Science and Technology Facilities Council (UK), the Royal Society (UK), the European Union's Horizon 2020 research and innovation programme under the Marie Skłodowska-Curie grant agreements No. 101006726, No. 734303, the National Natural Science Foundation of China

(Grant No. 11975153, 12075151), MSIP, NRF and IBS-R017-D1 (Republic of Korea), the German Research Foundation (DFG) through the Cluster of Excellence PRISMA+ (EXC 2118/1, Project ID 39083149).

References

1. W. E. Lamb, R. C. Retherford, Phys. Rev. 72 (1947) 241–243. doi:10.1103/PhysRev.72.241.

2. P. Kusch, H. M. Foley, Phys. Rev. 72 (1947) 1256–1257.

3. P. Kusch, H. M. Foley, Phys. Rev. 74 (1948) 250–263. doi:10.1103/PhysRev.74.250.

4. T. Aoyama, et al., Phys. Rept. 887 (2020) 1–166. arXiv:2006.04822.

5. B. Abi, et al., Phys. Rev. Lett. 126 (14) (2021) 141801. arXiv:2104.03281.

6. G. W. Bennett, et al., Phys. Rev. D 73 (2006) 072003.

7. S. Borsanyi, et al., Nature 593 (7857) (2021) 51–55. arXiv:2002.12347.

8. J. D. Jackson, 3rd Edition, Wiley, New York, NY, 1999.

9. J. Bailey, et al., Nucl. Phys. B 150 (1979) 1–75.

10. J. Kaspar, A. Fienberg, D. Hertzog, M. Huehn, P. Kammel, K. Khaw, D. Peterson, M. Smith, T. V. Wechel, A. Chapelain, L. Gibbons, D. Sweigart, C. Ferrari, A. Fioretti, C. Gabbanini, G. Venanzoni, M. Iacovacci, S. Mastroianni, K. Giovanetti, W. Gohn, T. Gorringe, D. Pocanic, Design and performance of sipm-based readout of pbf_2 crystals for high-rate, precision timing applications, Journal of Instrumentation 12 (01) (2017) P01009.
URL `http://stacks.iop.org/1748-0221/12/i=01/a=P01009`

11. A. Anastasi, et al., JINST 14 (2019) P11025. arXiv:1906.08432.

12. T. Albahri, et al., Phys. Rev. D 103 (2021) 072002.

13. T. Albahri, et al., Phys. Rev. A 103 (2021) 042208.

14. A. Keshavarzi, W. J. Marciano, M. Passera, A. Sirlin, Phys. Rev. D 102 (3) (2020) 033002. arXiv:2006.12666.

15. M. Cè et al. https://arxiv.org/pdf/2206.06582.pdf;

16. C. Aleaxndrou et al. https://arxiv.org/pdf/2206.15084.pdf;

17. C. Lehner (on behalf of RBC & UKQCD collaborations), "The hadronic vacuum polarization", Talk at Fifth Plenary Workshop of the Muon g-2 Theory Initiative, https://indico.ph.ed.ac.uk/event/112/contributions/1660/attachments/1000/1391/talk-nobackup.pdf;